„Babeş-Bolyai" University, Cluj-Napoca
Faculty of Mathematics and Computer Science
Department of Mathematics

Mathematical models and numerical simulations for the blood flow

SUMMARY OF PHD THESIS

Scientific Advisor
Prof. dr. univ. Titus Petrila

PhD Student
Balázs Albert

Cluj-Napoca, 2014

Table of Contents

Key words: blood flow, Cross type Non-Newtonian model, viscoelasticity, generalized Maxwell model for viscoelasticity, numerical simulation, artery with stenosis, artery with aneurysm, Internal Carotid Artery with stenosis, Abdominal Aortic Aneurysm, wall shear stress, rupture risk of artery with aneurysm, global rupture risk

Introduction

The physiology of the cardiovascular system was studied and clarified step by step through many centuries. The role of the blood vessels have already been identified in the antiquity, when it was realized that the arteries and veins have different roles.

In the 17th century, Sir William Harvey made some "modern" cardiovascular researches, and noticed that the blood flow in the vessels has a circulatory character. In the following century Euler and D. Bernoulli brought important contributions to the fluid dynamics with applications in hemodynamics too.

The French physician Poiseuille was the first, in 1844, who tried to understand the dynamics of the blood circulation. His results were completed by those of Reynolds (1883).

Later T. Young made some fundamental researches concerning the elasticity of the arterial tissues and the propagation of blood pressure. At the beginning of the 20th century, O. Frank set up an idea based on the analogy between the circulatory system and electric network [74].

In the past decade, the application of mathematical models, seconded by the use of efficient and accurate numerical algorithms, has made impressive progress in the interpretation of the circulatory system functionality, in both normal physiological and pathological situations, as well as in the perspective of providing patient appropriate design indications to specific surgical planning.

This new perspective has called for the development of a new field of fluid biomechanics and of applied mathematics. Although many substantial achievements have been made in the field of modeling, mathematical and numerical analysis, and scientific computation, where a variety of new concepts and mathematical techniques have been introduced, most of the difficulties are still on the ground and represent major challenges for the upcoming years.

The fact that blood exhibits non – Newtonian behavior was actually first recognized around the turn of the century (Enderle et al. 2000 [25]). Blood is a non-homogeneous, anisotropic, composite fluid, composed of a suspension of many asymmetric, relatively large, viscoelastic particles carried in a liquid.

Ronald L. Fournier (1998) [31] analyzed the blood from rheological point of view. He expected that the rheological behavior of blood to be some what more complex than a simple fluid (such as water for instance)

Ishikawa et al. (1998) [43] found that the non-Newtonian, pulsatile flow through a stenosed tube is different from Newtonian flow. The non-Newtonian property strengthens the peaks of wall shear stress and wall pressure, while it weakens the strength of the vortex.

Chakravarty and Mandal (1994) [13] studied analytically the unsteady flow behavior of blood in an artery under stenotic condition, by considering the blood to be a non-Newtonian fluid taking into account also the viscoelasticity of the blood. Mandal (2005) [50] pointed out that in some disease conditions, for example, patients with severe myocardial infarction, cerebrovascular diseases and hypertension, blood exhibits non-Newtonian properties.

Gijsen et al. (1999) [34] studied the impact of non-Newtonian properties of blood on the velocity distribution. They made a comparison between the non-Newtonian fluid model and a Newtonian fluid at different Reynolds numbers. Comparison reveals that the character of flow of the non-Newtonian fluid is simulated quite well by using the appropriate Reynolds number.

As an initial study, Formaggia et al. (2003) [29] and Lee and Xu (2002) [49] analyzed the blood flow behaviour in non-stenotic vessels or a normal arteries. A great number of theoretical studies related to blood flow through stenosed arteries have been carried out recently. In most of the studies carried out so far, the presence of “mild” (or single stenosis) was considered. Chakravarty and Mandal (1996) [14], noted that the problem becomes more acute in the presence of an “overlapping” stenosis (two or more stenoses one after the other) in the artery instead of having a “mild” stenosis.

There are different methods of solution in approaching the problem of blood flow in normal and stenosed artery. Some researchers tried to solve analytically but majority of them used numerical methods. Gerrald and Taylor (1977) [84] used the finite difference method (FDM) to solve the problem of blood flow in a normal artery. The finite difference method based on the central difference approximation has been also employed by Chakravarty and Mandal (1994) [13] and Mandal (2005) [50]. Misra and Pal (1999) [53] observed the blood motion using Crank-Nicolson implicit

finite difference method. Runge-Kutta formula has been used by Chakravarty and Mandal (1996, 2000) [15].

Beside the finite difference schemes, the finite element method has also been employed. Sud and Sekhon (1986) [82] used the finite element method (FEM) to model the blood flow in the case of a stenosed artery. Formaggia et al. (2003) [29] presented a finite element Taylor-Galerkin scheme to carry out several test cases.

The aim of the present PhD thesis is to simulate de blood flow in large blood vessels (arteries), taking into consideration the non-Newtonian character of the blood together with the viscoelastic behavior of the vessels wall where the flow takes place. The accent is put on the simulations in different pathological cases, when the blood vessel has a stenosis (a weakening of the vessel diameter) or when it has an aneurysm (a dilatation of the vessel). The numerical simulations were made using the COMSOL Multiphysics 3.3 package, which is based on the finite element method (FEM).

To validate the obtained results, these were compared to the results obtained already by other researchers [54], [58], [52], [28], [94].

Some of the results were exported in video extension; these results are attached to the present thesis on a CD, according to Appendix 2.

Original results and contributions:

The elaboration of a Cross type non-Newtonian mathematical model for the blood flow in large vessels, attached by a generalized Maxwell model describing the viscoelastic behavior of the blood vessel. These mathematical models are presented in Chapter 5 and Chapter 6, and were published in the paper **Albert, B.**, Vacaras, V., Trif, D., Petrila, T., Non-Newtonian approach of the blood flow in large viscoelastic vessels with stenosis or aneurysm, Jokull Journal, vol. 63, No. 7, pp. 160-173, 2013 [3].

The realization of a number of numerical simulations for the blood flow in arteries with different stenoses (published in the papers Petrila T., **Albert B.**, Calculation of the Wall Shear Stress in the Case of a Stenosed Internal Carotid Artery, Indian Journal of Applied Research, Vol. 3, No. 9, pp. 396-398, 2013 [67] and Petrila T., **Albert B.**, Calculation of the Wall Shear Stress in the case of an Internal Carotid Artery with stenoses of different sizes, INCAS Buletin, Vol. 5, Special Issue, 15-22, 2014 [66]) or in arteries with different aneurysms (published in **Albert B.**, Vacaras V., Petrila T., Calculation of the Wall Shear Stress in the Case of an Abdominal

Aortic Aneurysm, Wulfenia, vol. 20, No.12, pp. 159-168, 2013 [4]). The results of these simulations are presented in Chapter 8, sections 8.4, 8.5, 8.5.1.

The deduction of a global condition for the rupture risk of the vessel wall in the case of an artery with aneurysm, and the application of this condition in the case of an abdominal aortic aneurysm with a double aneurysm (see Chapter 8, sections 8.6, 8.6.1). These results are presented in the paper **Albert B.**, Vacaras V., Deac D., Petrila T., A global condition for the rupture risk of an Abdominal Aortic Aneurysm (AAA) obtained within a mathematical and numerical model for blood flow in large vessels, accepted to be published in Jokull Journal [5].

The PhD thesis is structured as follows:

Chapter 1 contains an introductory part about the evolution of the researches made in the field of the blood flow in the cardiovascular system. In this chapter are presented some characteristics of the blood and the blood vessels as well.

In the Second chapter one introduced the notions of stenosis and aneurysm from a medical point of view. The formation and the effects of them are described correspondingly.

More mathematical functions, modeling different stenoses shapes are presented in Chapter 3. The “mild” stenosis, “cosine-shaped” stenosis, “bell-shaped” stenosis, irregular stenosis, multiple stenoses are mentioned.

In Chapter 4 the basic concepts for the description of the fluid flow are presented, successively the continuity equation, the Navier-Stokes equations, the use of the Fourier series to describe pulsatile flow conditions, the Womersley analytic solution for the pulsatile flow in a rigid tube are presented.

In the first section of Chapter 5 the Newtonian model for the blood flow in large arteries is described, then, in Section 5.2, the deduction of a non-Newtonian model is presented. This last model is used for the upcoming numerical simulations.

In Chapter 6 some mathematical models considered for describing the viscoelastic behavior of the vessel wall are presented. The generalized Maxwell model is pointed out, which would be used by us later on for the vessel wall behavior.

The steps to be followed, how such a model should be built in COMSOL 3.3, are described in Chapter7. Starting from the selection of the corresponding modules for the fluid (blood) and the structure (vessel wall), through the building of the geometry, through the setting of the used coefficients, through the definition of the initial and boundary conditions, through the generation of the domain mesh, until the

setting of the solver parameters, they are the steps which are correspondingly presented.

Chapter 8 contains the results of the numerical simulations. The first results are obtained for the blood flow (using both the Newtonian and non-Newtonian model) in an artery with a stenosis and then in an artery with an aneurysm, in both cases the vessel wall being considered to be elastic. Continuing with the case when, beside the non-Newtonian (Cross type) model for the blood, the viscoelastic behavior of the wall is also considered. Section 8.4 presents the obtained results for an Internal Carotid Artery with a stenosis (a real medical case). The accent is put on the calculation of the wall shear stress (*WSS*), which could be responsible for the possible rupture of the vessel wall. In Sections 8.5 and 8.6 some results obtained for arteries with aneurysms are presented. In the case of the aneurysms the real medical case of an abdominal aortic aneurysm was examined in detail.

1. Blood and blood vessels

1.1. Blood

Blood is a bodily fluid that delivers necessary substances such as nutrients and oxygen to the cells and transports metabolic waste products away from those same cells. It is composed of blood cells suspended in blood plasma. Plasma, which constitutes 55% of blood fluid, is mostly water (92% by volume), and contains dissipated proteins, glucose, mineral ions, hormones and blood cells themselves. The blood cells are mainly red blood cells (also called RBCs or erythrocytes) and white blood cells, including leukocytes and platelets.

The principal quantities which describe blood flow are the *velocity* **u** and *pressure P*. In the fluid-structure interaction problems, the *displacement* of the vessel wall due to the action of the flow field is another relevant quantity. Pressure, velocity and vessel wall displacement will be functions of time and the spatial position.

1.2. Blood vessels

There are three major types of blood vessels: the arteries, which carry the blood away from the heart; the capillaries, which enable the actual exchange of water and chemicals between the blood and the tissues; and the veins, which carry blood from the capillaries back toward the heart.

The wall of large blood vessels has a circumferentially layered structure. The most important layers are: the internal, thin *intima*, which is composed of the inner *endothelium*, the *internal elastic lamina*, the middle muscular *media*, the external elastic lamina and the outer *adventitia*.

2. Stenosis and Aneurysm

Atherosclerosis occurs when the nature of blood flow changes from its usual state to a disturbed flow condition due to the presence of a stenosis in an artery. Stenosis is defined as a partial occlusion of the vessels caused by abnormal growth of tissues or the deposition of cholesterol as other substances on the arterial wall.

Signs and symptoms usually come out when the severe blockage impedes blood flow to different organs. Most of the time, patients realize that they have the disease only when they experience other cardio vascular disorders such as stroke or heart attack.

Risk factors:

- obesity;
- unequilibred diet;
- sedentary life stile;
- smoking;
- diabetes;
- alcoholism;
- hyperlipoproteinemia and arterial hypertension.

An aortic aneurysm is a general term for an enlargement (dilatation) of the aorta. While the cause of an aneurysm may be multifactorial, the end result is an underlying weakness in the wall of the aorta at that location. When rupture occurs, massive internal hemorrhage results, and, unless treated immediately, shock and death can occur within minutes to hours.

There are two types of aortic aneurysms: the abdominal aortic aneurysm and the thoracic aortic aneurysm. In figure 2.1 an abdominal aortic aneurysm is presented (*AAA*), the image has been got by abdominal ecography at the Neurology Clinic, Cluj-Napoca.

Causes of abdominal and thoracic aortic aneurysms

- atherosclerosis;
- genetic factors – up to 28% of the persons who present aortic aneurysm have a member in their family with the same affection;
- age, the aorta loses its elasticity throughout the years and becomes more rigid;

- infections, such as Syphilitic aortitis [59];
- traumatisms, violent shots in the chest or in the abdomen.

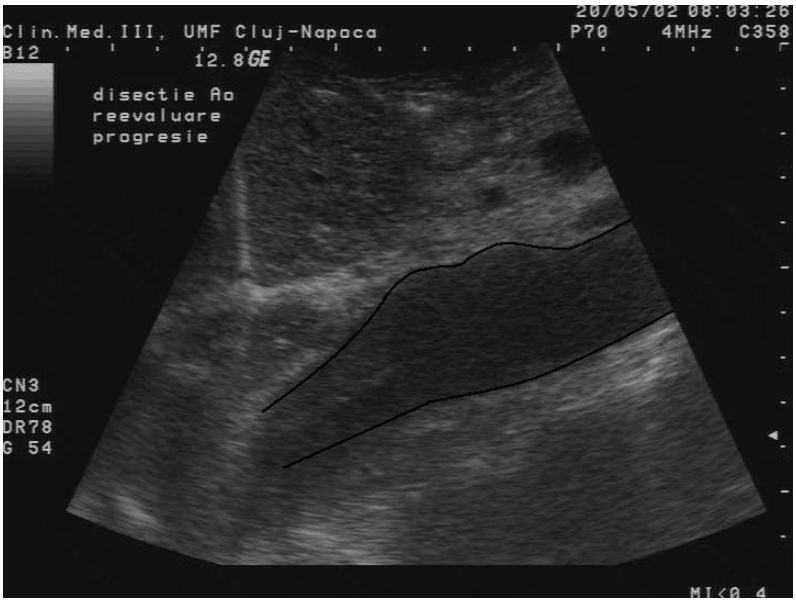

Figure 2.1 Image of a real abdominal aortic aneurysm

3. The geometry of the stenosis

For the stenosis a number of types of "geometries" can be defined from mathematical point of view (Zuhaila, 2006 [102]).

In this chapter we are mentioning the vessel with constant radius (without stenosis), "mild" stenosis, "cosine-shaped" stenosis, "bell-shaped" stenosis, irregular stenosis, multiple stenosis.

4. Mathematical description of the fluid flow

To express the velocity in terms of three Cartesian coordinates means that velocity becomes a function of *x*, *y*, and *z* spatial coordinates, as well as a function of time. By using *u, v*, and *w* for the velocity components in the *x*, *y*, and *z* directions, respectively, in a concise form it can be written

$$\mathbf{u}(x,y,z,t) = u\vec{i} + v\vec{j} + w\vec{k} = u(x,y,z,t)\vec{i} + v(x,y,z,t)\vec{j} + w(x,y,z,t)\vec{k},$$

where $\vec{i}$, $\vec{j}$ and $\vec{k}$ are the unit vectors in the directions of *x*, *y* and *z* respectively.

For the acceleration we may also write

$$\vec{a}(x,y,z,t) = a_x\vec{i} + a_y\vec{j} + a_z\vec{k} = \frac{\partial \mathbf{u}}{\partial t} + u\frac{\partial \mathbf{u}}{\partial x} + v\frac{\partial \mathbf{u}}{\partial y} + w\frac{\partial \mathbf{u}}{\partial z},$$

where a_x, a_y and a_z are the Cartesian components of the acceleration.

It is possible to express the acceleration more concisely

$$\vec{a} = \frac{D\mathbf{u}}{Dt},$$

where the operator $\frac{D()}{Dt}$ is the material derivative.

Defining the gradient operator, $\vec{\nabla}()$, $\vec{\nabla}() = \frac{\partial()}{\partial x}\vec{i} + \frac{\partial()}{\partial y}\vec{j} + \frac{\partial()}{\partial z}\vec{k}$ we can rewrite the material operator in the form of

$$\frac{D()}{Dt} = \frac{\partial()}{\partial t} + \mathbf{u}\cdot\vec{\nabla}().$$

Let us introduce the Laplace operator, which is the scalar product of the gradient operator with itself, namely

$$\nabla^2() = \vec{\nabla}()\cdot\vec{\nabla}(), \text{ or}$$

$$\nabla^2() = \frac{\partial^2()}{\partial x^2} + \frac{\partial^2()}{\partial y^2} + \frac{\partial^2()}{\partial z^2}.$$

4.1. The Continuity Equation

The continuity equation, or the mass conservation, can be written in our case as $\rho_1 A_1 V_1 = \rho_2 A_2 V_2 = \text{constant}$, where ρ is the fluid density, A is the transversal sectional area of the blood vessel, V is the average velocity of the blood through the cross section.

The more general form of the continuity equation is

$$\frac{\partial \rho}{\partial t} + \frac{\partial (\rho u)}{\partial x} + \frac{\partial (\rho v)}{\partial y} + \frac{\partial (\rho w)}{\partial z} = 0 .$$

In the case of the incompressible fluids, as blood is, the density being constant, the continuity equation can be simplified to

$$\frac{\partial u}{\partial x} + \frac{\partial v}{\partial y} + \frac{\partial w}{\partial z} = 0 .$$

This equation can be also written as $div\mathbf{u} = 0$.

4.2. Representation with Fourier series of the attached conditions

For the case of pulsatile flow in a tube with axial symmetry, where **u** is velocity and P is pressure, the partial derivative of velocity **u** with respect to time is not zero. In addition the partial derivative of pressure P with respect to z (the distance along the tube) is also nonzero, namely

$$\frac{\partial \mathbf{u}}{\partial t} \neq 0 \text{ and } \frac{\partial P}{\partial z} \neq 0 .$$

Since the pressure wave form is periodic, it is convenient to write the partial derivative of pressure $\partial P / \partial z$ by using a Fourier series.

This periodic function depends on the fundamental frequency of the signal ω (heart rate in rad/s) and the time t. We can write such a function as a sum of sine and cosine terms, with appropriate coefficients, known as Fourier coefficients.

$$\frac{\partial P}{\partial z} = A_0 + A_1 \cos(\omega t) + A_2 \cos(2\omega t) + A_3 \cos(3\omega t) + \ldots + B_1 \sin(\omega t) + B_2 \sin(2\omega t) + B_3 \sin(3\omega t) + \ldots$$

This is a Fourier series representation of the pressure gradient. To obtain the Fourier coefficients A_0, A_1, A_2, ..., B_1, B_2, ... the most known method consists in the evaluation of a series of integrals. For a periodic function f with period T_0, we have

$$A_0 = \frac{1}{T_0}\int_0^{T_0} f(t)dt$$

$$A_n = \frac{2}{T_0}\int_0^{T_0} f(t)\cos(n\omega t)dt$$

$$B_n = \frac{2}{T_0}\int_0^{T_0} f(t)\sin(n\omega t)dt\ .$$

To get effectively the values of such integrals can be very difficult if *f* is other than a fairly simple function. That is why it may be convenient to evaluate these integrals numerically.

4.3. Navier-Stokes equations

These equations are, second-order, partial differential equations and they are considered to be the governing differential equations of motion for incompressible, Newtonian fluids.

The Navier-Stokes equations, in gravitational field, can be written rather efficiently in the following form

$$\rho\frac{D\mathbf{u}}{Dt} = \rho\vec{g} - \vec{\nabla}P + \mu\nabla^2\mathbf{u}\,,$$

where, ρ is the fluid density, $\frac{D\mathbf{u}}{Dt}$ is the material derivative of the fluid velocity, $\vec{g}$ is the gravitational acceleration, $\vec{\nabla}P$ represents the pressure gradient, while μ represents the viscosity of the fluid.

4.4. Pulsatile flow in rigid tube. The Womersley solution

Let us assume a Newtonian fluid, uniform, laminar, axially symmetric, pipe flow. This is similar to the Poiseuille flow problem, but now we are considering pulsatile flow rather than steady.

For the pressure gradient we use the Fourier series representation

$$\frac{\partial P}{\partial z} = \mathrm{Re}\left\{\sum_{n=0}^{\infty} a_n e^{in\omega t}\right\}.$$

Therefore, for each harmonic *n*, we can write each component of the driving pressure as a complex exponential.

$$\left.\frac{\partial P}{\partial z}\right|_n = a_n e^{in\omega t}.$$

We use now the scalar form of the Navier-Stokes equation

$$\rho\frac{\partial u}{\partial t}+\rho\left(w\frac{\partial u}{\partial z}+v_r\frac{\partial u}{\partial r}+\frac{v_\theta}{r}\frac{\partial u}{\partial \theta}\right)=\rho g_z-\frac{\partial P}{\partial z}+\mu\left(\frac{\partial^2 u}{\partial z^2}+\frac{\partial^2 u}{\partial r^2}+\frac{1}{r}\frac{\partial u}{\partial r}+\frac{1}{r^2}\frac{\partial^2 u}{\partial \theta^2}\right).$$

Since the flow is axially symmetric, there is no swirling flow and no velocity in the radial or transverse directions and therefore no change in velocity in either the radial or transverse direction, so $\frac{\partial u}{\partial \theta}=0$, $v_r=0$ and $v_\theta=0$. Since the flow is uniform, there is no change for velocity u in the z (axial) direction, so that $\frac{\partial u}{\partial z}=0$. The flow is also horizontal; therefore the Navier-Stokes equation simplifies

$$\rho\frac{\partial u}{\partial t}=-\frac{\partial P}{\partial z}+\mu\left(\frac{\partial^2 u}{\partial r^2}+\frac{1}{r}\frac{\partial u}{\partial r}\right).$$

Dividing this equation by ρ, introducing the kinetic viscosity $\nu=\frac{\mu}{\rho}$ and replacing $\left.\frac{\partial P}{\partial z}\right|_n = a_n e^{in\omega t}$, we arrive to the following equation

$$\frac{a_n e^{in\omega t}}{\rho}=\nu\left(\frac{\partial^2 u_n}{\partial r^2}+\frac{1}{r}\frac{\partial u_n}{\partial r}\right)-\frac{\partial u_n}{\partial t}.$$

This is a linear, second-order, partial differential equation (PDE).

The corresponding velocity, which satisfies the above PDE is

$$u_n=\mathrm{Re}\left\{\frac{a_n}{in\rho\omega}\left[\frac{J_0(\lambda r)}{J_0(\lambda R)}-1\right]e^{in\omega t}\right\}.$$

where J_0 is a zero-order Bessel function of the first kind, $\lambda^2=\frac{i^3 n\omega}{\nu}$, ν is the kinetic viscosity, while ω is the frequency.

Now to find the velocity as a function of radius r and time t for the entire driving pressure, we put together the steady flow result u_0 with the results from all harmonics, i.e., (Womersely, 1955 [**Error! Reference source not found.**])

$$u(r,t)=u_0(r)+\sum_{n=1}^{\infty}u_n(r,t).$$

A quantity that is a bit more important than the velocity. It is the flow rate passing through a given cross section of the blood vessel. To find this flow rate one needs only to integrate the just found velocity function multiplied by the differential area, over the entire cross section. The differential area, a simple annulus, may be written as a function of *r*, that is, $2\pi r dr$, so the flow rate becomes

$$Q(t) = \int_0^R u(r,t) \cdot 2\pi r dr .$$

Using the integral identity $\int x J_0(x) dx = x J_1(x)$ for the Bessel functions, where J_1 denotes a Bessel function of the first kind and of the first order, we reach a solution for the flow rate produced by harmonic *n* of the pressure gradient

$$Q_n = (\pi R^2)\,\mathrm{Re}\left\{ \frac{a_n}{in\rho\omega} \left[\frac{2J_1(\lambda R)}{\lambda R J_0(\lambda R)} - 1 \right] e^{in\omega t} \right\}.$$

These must be summed and added to

$$Q_0 = a_0 \frac{8\mu}{\pi R^4},$$

which is the average flow rate produced by the constant term. Finally we have

$$Q(t) = Q_0 + \sum_{n=1}^{\infty} Q_n(t) .$$

Measuring the flow rate of the blood in a given section (which can be made in medical laboratories), using the Womersley solution, one can calculate the values of the velocity and pressure in that given section.

When I tried to implement the Womersley model in COMSOL 3.3, I met some difficulties. That is because, the Womersley solution can be used only in ideal conditions, namely; when the flow is laminar, the fluid is Newtonian, and the tube is straight (cylindrical) and rigid.

5. Mathematical models for the blood flow in large vessels

5.1. Newtonian model

Firstly we are proposing a mathematical model, in which we have used for the blood flow in large vessels the Stokes system for incompressible fluid. At the same time we admit the incompressibility and homogeneity of the blood while its flow is laminar and the exterior body forces are neglected. Then the vessel wall is considered to be elastic.

5.2. Non-Newtonian model

We accept a non-Newtonian rheological representation for blood, with a variable coefficient of viscosity under the conditions of an unsteady (pulsatile) flow regime connected with the rhythmic pumping of the blood by the heart. We admit again the incompressibility and homogeneity of the blood while its flow is laminar and the exterior body forces are neglected.

In the case of the non-Newtonian model the viscosity coefficient is a function of the shear rate ($\dot{\gamma}$), $\mu = \mu(\dot{\gamma})$. We mention some of the rheological models elaborated and proposed for the blood flow:

- Power law model

$\mu(\dot{\gamma}) = k\dot{\gamma}^{n-1}$

- Powell-Eyring Model

$\mu(\dot{\gamma}) = \frac{\sinh^{-1}(\lambda\dot{\gamma})}{\lambda\dot{\gamma}},\ \lambda = 5{,}383s$

- Cross Model

$\mu(\dot{\gamma}) = (1+(\lambda\dot{\gamma})^m)^{-1},\ \lambda = 1{,}007s,\ m = 1{,}028$

- Modified Cross Model 1

$\mu(\dot{\gamma}) = (1+(\lambda\dot{\gamma})^m)^{-a},\ \lambda = 3{,}736s,\ m = 2{,}406,\ a = 0.254$

- Modified Cross Model 2 (Ohta et al., 2005 [54])

$\mu(\dot{\gamma}) = \mu_\infty + (\mu_0 - \mu_\infty)(1+(\dot{\gamma}/C)^m)^{-1}, \mu_\infty = 0{,}0035Pa.s,$

$\mu_0 = 0{,}0364Pa.s,\ m = 1{,}45,\ C = 2{,}63\ s^{-1}$

- Carreau Model

$\mu(\dot{\gamma}) = (1 + (\lambda\dot{\gamma})^2)^{(n-1)/2}$, $\lambda = 3{,}313s$, $n = 0{,}3568$

- Carreau-Yasuda Model

$\mu(\dot{\gamma}) = (1 + (\lambda\dot{\gamma})^a)^{(n-1)/a}$, $\lambda = 1{,}902s$, $n = 0{,}22$, $a = 1{,}25$

where λ is the so called „relaxation" time, k is a time constant for the shear thinning behavior, n is the index for a shear thinning behavior, m is the so called Cross constant (Galdi et al., 2008 [37]).

We use the Navier-Stokes equation in the following form

$$\rho\left(\frac{\partial \mathbf{u}}{\partial t} + \mathbf{u}\cdot\nabla\mathbf{u}\right) = -\nabla p + \mu(\dot{\gamma})(\nabla^2\mathbf{u}),$$

where **u** is the blood velocity vector, p is the blood pressure, ρ is the blood density, the viscosity of the blood is given by the Cross model $\mu(\dot{\gamma}) = \mu_s + \frac{\mu_0^*}{1 + (k\dot{\gamma})^{1-n}}$. μ_s and μ_0^* being some viscosity coefficients of the blood.

5.3. Initial and boundary conditions

The above evolution equations are joined to some boundary conditions which express the existence of a pressure gradient along Oz axis according to the heart beats and implicitly to the rhythmic blood pushing into the vessel (feature which is important in large vessel).

At $r = R$, due to the viscoelastic behavior of the vessel's wall, the velocity of the blood must be equal to the displacement velocity of the wall. The boundary conditions at "edges" $z = 0$ and $z = L$ of the vessel agree with a physiological pulse velocity given by a periodic time-varying function.

5.4. *Improved model*

In order to mimic the heart beats, on the input boundary $z = 0$ we have accepted an oscillatory physiological velocity profile (1second periodic function)

$$u = 0,\ v = F(t)\cdot\left(1-\left(\frac{r}{R}\right)^2\right).$$

Here $F(t) = \frac{a_0}{2} + \sum_{m=1}^{7}(a_m \cos(2\pi mt) + b_m \sin(2\pi mt))$, with the coefficients

$$a_0 = 2{,}5962\cdot 10^{-5},$$
$$a_1 = -0{,}3577\cdot 10^{-5},\ b_1 = -0{,}5384\cdot 10^{-5},$$
$$a_2 = -0{,}2380\cdot 10^{-5},\ b_2 = 0{,}5379\cdot 10^{-5},$$
$$a_3 = 0{,}5564\cdot 10^{-5},\ b_3 = -0{,}1866\cdot 10^{-5},$$
$$a_4 = -0{,}2718\cdot 10^{-5},\ b_4 = -0{,}0748\cdot 10^{-5},$$
$$a_5 = -0{,}0619\cdot 10^{-5},\ b_5 = 0{,}1086\cdot 10^{-5},$$
$$a_6 = 0{,}1386\cdot 10^{-5},\ b_6 = 0{,}0634\cdot 10^{-5}$$
$$a_7 = -0{,}0618\cdot 10^{-5},\ b_7 = -0{,}1194\cdot 10^{-5}.$$

giving a velocity profile similar to that used by Finol and Amon, 2003 [27], see figure 5.1. From this flow rate profile we established the velocity profile considered for the blood flow.

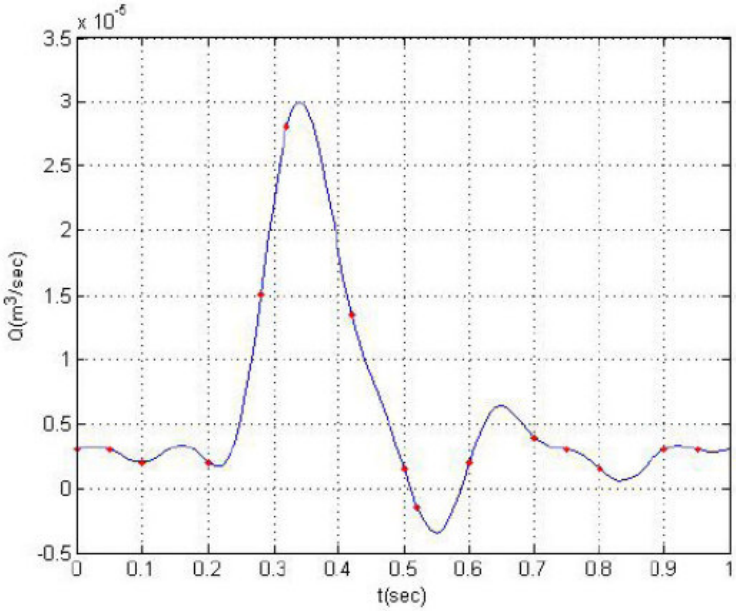

Figure 5.1 Pulsatile volumetric flow rate

6. Mechanics of the viscoelastic wall

Pulsatile flows in a flexible tube can significantly deform its wall. Deformations are determined by the material's properties and depend on the amplitude of the pressure pulse.

Unlike purely elastic materials, a viscoelastic substance has an elastic component and a viscous component. The viscosity of a viscoelastic substance gives to the material a strain rate dependence on time.

Experimental data demonstrates that the wall of the blood vessel has a viscoelastic behavior, as can be found in the works of Gineau [35] and Saito [79].

Linear viscoelastic models

The Kelvin-Voigt model

The simplest model of viscoelastic materials is linear and consist in adding elastic and viscous stresses

$$\sigma = \sigma_e + \sigma_v = E\varepsilon + \mu \frac{\partial \varepsilon}{\partial t},$$

where E is the elastic modulus, μ is the viscosity of the wall, while ε is the deformation of the wall.

The Maxwell model

Another widely used model for viscoelastic materials is the Maxwell model. The mathematical low for this model is

$$\frac{\partial \varepsilon}{\partial t} = \frac{\partial \varepsilon_e}{\partial t} + \frac{\partial \varepsilon_v}{\partial t},$$

where $\varepsilon_e = \frac{\sigma}{E}$ elastic component of the deformation while $\frac{\partial \varepsilon_v}{\partial t} = \frac{\sigma}{\mu}$ is the time derivative of the viscous component of the deformation. Thus we obtain the following law

$$\frac{\partial \varepsilon}{\partial t} = \frac{1}{E}\frac{\partial \sigma}{\partial t} + \frac{\sigma}{\mu}.$$

The generalized Maxwell model

The generalized Maxwell model (or Maxwell-Wiechart model) is the more general form for the linear viscoelastic behavior. It takes into account that the relaxation of the wall does not occur at a single moment, but at a distribution of moments. Due to molecular segments of different lengths, with shorter ones contributing less than the longer ones, there is a varying time distribution.

More precisely, the linear viscoelastic material models can be expressed by integral-equation

$$\sigma = \int_0^t G(t)\frac{\partial \varepsilon}{\partial t} dt$$

where σ is the stress, ε is the strain and *G(t)* is the relaxation modulus function and it can be considered as the stress when the material is held at a constant strain.

7. Implementation of the model in COMSOL 3.3

We start with the selection of the corresponding modules for the fluid (*non-Newtonian module*) and for the vessel wall (*axial symmetry stress-strain module*). After the creation of the domain geometry, the steps for the setting of the used coefficients are presented. Further the initial and the boundary conditions for the fluid (blood) and for the solid (vessel wall) are set up. Finally the domain mesh is generated and the settings for the solver parameters are made.

8. Numerical results

In this Chapter all our original results are presented, results obtained through numerical simulations, based on the Cross type non-Newtonian model for the blood flow together with the generalized Maxwell model for the viscoelastic vessel wall.

The used Cross type rheological model has the following form

$$\mu(\dot{\gamma}) = \mu_s + \frac{\mu_0^*}{1 + k\dot{\gamma}^{1-n}},$$

where the values for the involved coefficients are: $\mu_s = 0{,}00345\, Pa.s$, $\mu_0^* = 0{,}0465\, Pa.s$, $k = 1{,}036$, $n = 0{,}2$ respectively.

For the beginning we accept an elastic behavior for the vessel wall, setting the Young modulus to $E = 1{,}0 \cdot 10^6\, Pa$ and the Poisson ratio to $\vartheta = 0{,}33$ (Gineau, 2010 [35]).

Let us consider an artery "segment" of radius $R = 0.005m$, length $L = 0.1m$, the thickness of the limiting wall being $0.001m$. The mass density of the blood has been fixed at $\rho = 1060 kg/m^3$.

Concerning the boundary conditions, in order to mimic the heart beats, on the input boundary $z = 0$ we have accepted an oscillatory physiological velocity profile (1 second periodic function)

$$v_{in} = F(t) \cdot \left(1 - \left(\frac{r}{R}\right)^2\right),$$

where $F(t) = \frac{a_0}{2} + \sum_{m=1}^{7} (a_m \cos(2\pi mt) + b_m \sin(2\pi mt))$ is a periodic function with the following coefficients

$$a_0 = 2{,}5962 \cdot 10^{-5},$$
$$a_1 = -0{,}3577 \cdot 10^{-5},\ b_1 = -0{,}5384 \cdot 10^{-5},$$
$$a_2 = -0{,}2380 \cdot 10^{-5},\ b_2 = 0{,}5379 \cdot 10^{-5},$$
$$a_3 = 0{,}5564 \cdot 10^{-5},\ b_3 = -0{,}1866 \cdot 10^{-5},$$
$$a_4 = -0{,}2718 \cdot 10^{-5},\ b_4 = -0{,}0748 \cdot 10^{-5},$$
$$a_5 = -0{,}0619 \cdot 10^{-5},\ b_5 = 0{,}1086 \cdot 10^{-5},$$
$$a_6 = 0{,}1386 \cdot 10^{-5},\ b_6 = 0{,}0634 \cdot 10^{-5}$$
$$a_7 = -0{,}0618 \cdot 10^{-5},\ b_7 = -0{,}1194 \cdot 10^{-5}$$

At the points of the vessel axis of symmetry r=0 we have imposed the axially symmetry requirements while on the vessel walls the velocity of the blood is equal to the displacement velocity of the vessel wall. In order to avoid the transient effect of the initial conditions, although the time integration interval is t∈ [0,20s], the results are presented only for the last 10 periods, t∈ [10,20s].

When the value of the shear rate ($\dot{\gamma}$) is between 10^{-2} 1/s and 10^{2} 1/s, the dependence on the viscosity is linear. In this interval the difference between the Newtonian and the non-Newtonian model is insignificant, but outside this interval the non-Newtonian model is more accurate for describing the blood flow in large vessels.

We have calculated the value of wall shear stress $WSS = \mu\left(\frac{\partial u}{\partial z} + \frac{\partial v}{\partial r}\right)$ in several particular points on the wall of a stenosed artery, this quantity being responsible for possible ruptures of the vessel wall (Ohta et al., 2005 [54] and Gasser et al., 2010 [32]).

8.1. Comparison of the Newtonian model with the non-Newtonian model

In this section we compared the results obtained using the Newtonian model with those got by the non-Newtonian model.

8.2. Viscoelastic model

Beginning with this chapter we take into consideration the viscoelasticity of the limiting walls. To describe the viscoelastic behavior of the vessel's wall we have used the generalized Maxwell model. The values of the material constants are $\mu_1 = 0{,}04$, $\mu_2 = 0{,}08$, $\mu_3 = 0{,}09$, $\mu_4 = 0{,}25$, $\mu_0 = 1-(\mu_1+\mu_2+\mu_3+\mu_4)$, $\lambda_1 = 0{,}02s$, $\lambda_2 = 0{,}3s$, $\lambda_3 = 3s$, $\lambda_4 = 12s$, after Craiem et al., 2008 [22].

The numerical simulations are made for an artery with stenosis and for an artery with aneurysm. The results are presented in the figures 8.1 and 8.2.

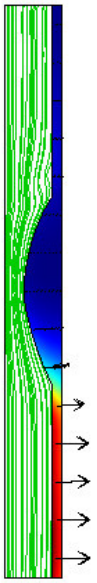

Figure 8.1 Artery with stenosis. Stream lines and the displacement of the wall at a given time (non-Newtonian, viscoelastic model)

Figure 8.2 Artery with aneurysm. Stream lines and the displacement of the wall at a given time (non-Newtonian, viscoelastic model)

8.3. *Improved initial conditions*

To obtain more realistic initial conditions - which are compatible with the used non-Newtonian model - at the inlet boundary of the arterial segment with stenosis or aneurysm we will make the following approach.

We have lengthened "theoretically" the envisaged arterial segments. At the inlet boundary (z = 0) of the whole arterial segment we have first imposed a parabolic profile for the velocity, as in the Newtonian case. Due to the evolution of the blood flow this artificial initial condition has been modified at the beginning of the arterial segment with stenonsis or aneurysm. The inlet velocity has not a parabolic profile anymore, it has now a realistic profile and the further simulations in the vicinity of the stenosis and the aneurysm are then made using these modified new initial conditions.

The modified velocity profiles are presented in figures 8.3 (stenosed artery) and 8.4 (artery with aneurysm)

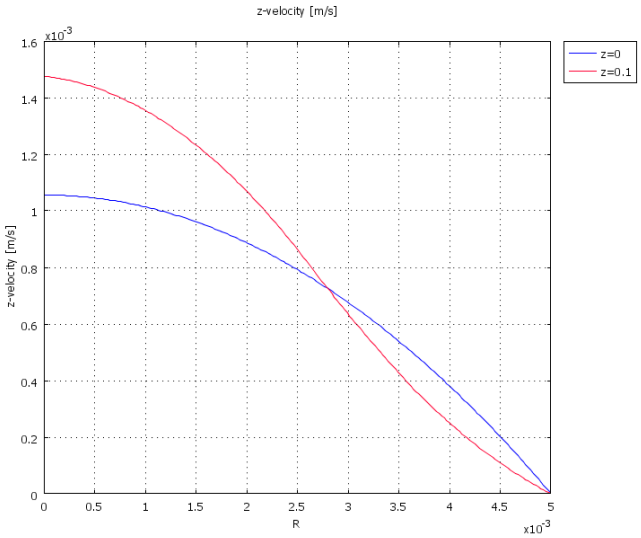

Figure 8.3 Velocity profile at the cross sections $z = 0$ and $z = 0.1$ in the case of stenosed artery

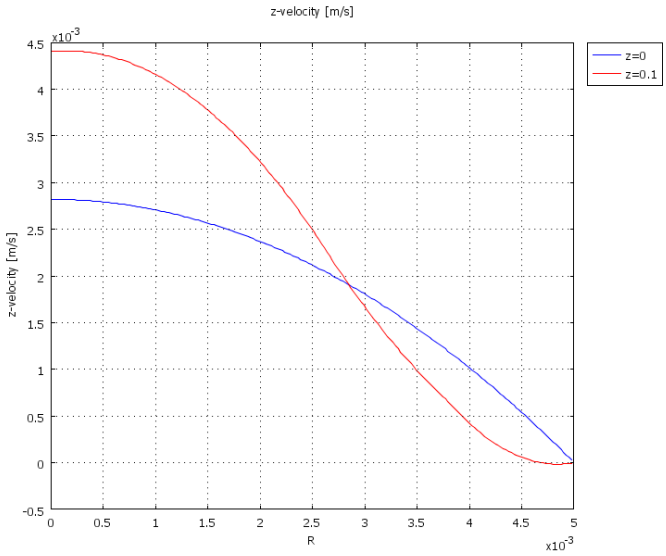

Figure 8.4 Velocity profile at the cross sections $z = 0$ and $z = 0.1$ in the case of artery with aneurysm

8.4. A real medical case

In this section we are presenting a real case of a stenosed artery. In figure 8.5 the velocity field of a human internal carotid artery (ICA), which has a stenosis of 69%, can be seen. To validate our numerical model presented above, we use the geometry of this ICA to get the corresponding numerical results by using our technique.

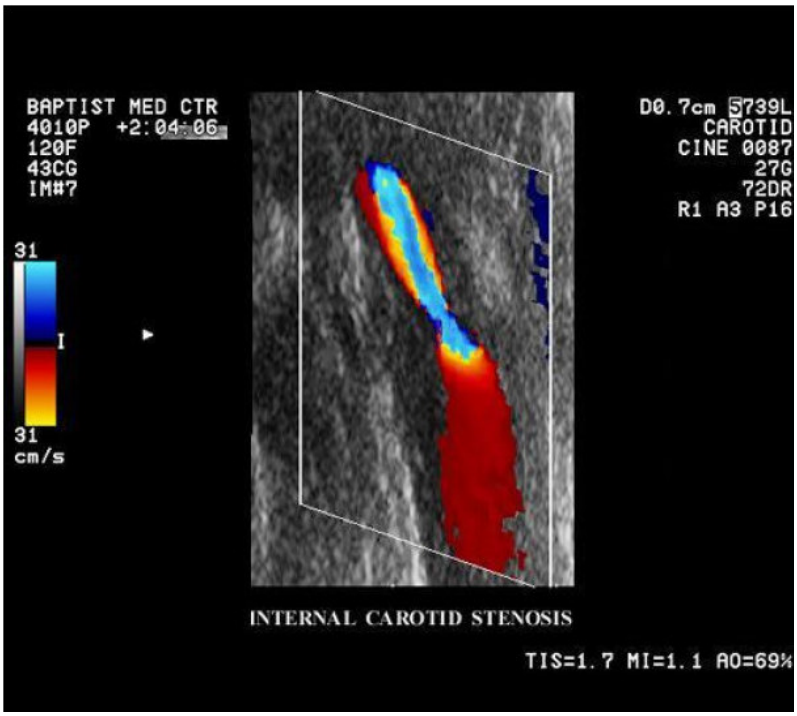

Figure 8.5 Velocity field of the blood in a stenosed ICA. Medical measuremet

The length of the stenosed arterial segment is 3*cm*, the internal diameter of the blood vessel is 7*mm*, the thickness of the vessel wall is 0.8*mm*. We are using the same Cross type non-Newtonian rheological model, with the same improved initial condition and with the same boundary conditions as in the previous section. The time integration interval is $t \in [0,10s]$ and the results are presented only for the last 5 periods, i.e., $t \in [5,10s]$.

The velocity field, at a certain time (t=8s) resulting from the numerical simulation is presented in figure 8.6. Comparing the figures 8.5 and 8.6 it shows up that the result obtained numerically coincides well with those got by laboratory measurement. We remark, that in figure 8.6 (got by COMSOL 3.3) the red color represents high velocities and blue color represents low velocities of the blood, while in figure 8.5 the meaning of the colors are inverted (due to the medical instruments), i.e., the results are in total agreement.

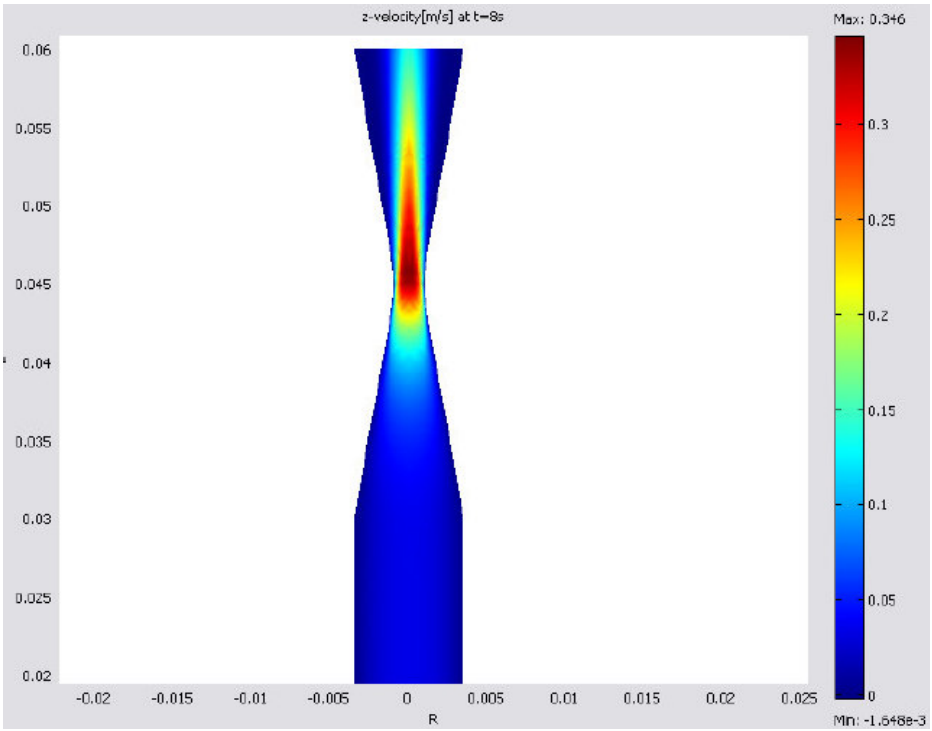

Figure 8.6 Velocity field of a stenosed ICA. Numerical result

We have chosen 4 particular points on the vessel wall of the stenosed ICA (see figure 8.7) in which the values of the *WSS* are evaluated.

In figure 8.8 the variation of the wall shear stress (through 5 seconds) – evaluated in those four particular points, is presented. It can be clearly seen, that the *WSS* reaches very high values in the middle of the stenosis (the red point on figure 8.7).

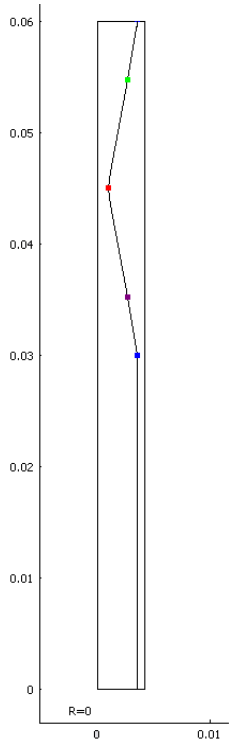

Figure 8.7 The 4 particular points on wall of the stenosed ICA

(coordinates on axes are expressed in *m*)

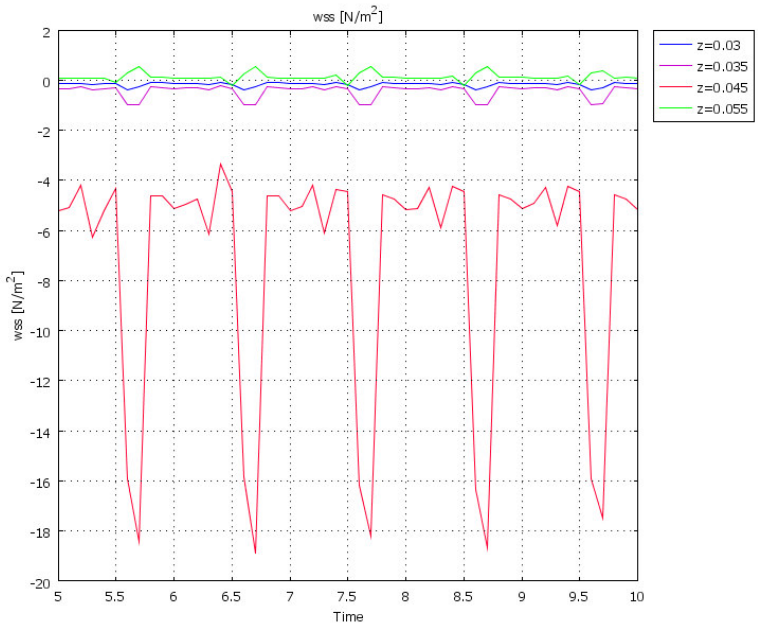

Figure 8.8. Values of the WSS (through 5 seconds) in the 4 particular points

Trying to make a connection between the values of the wall shear stress (*WSS*) – which is believed to have a special importance in the possible ruptures of vascular vessels – and the degree of the stenosis we examine numerically the same ICA in four cases: with a stenosis of 30%, 50%, 70% and 90% respectively. The results got for the values of the *WSS* in these four cases are compared.

In the case of the artery with a stenosis of 30 % the highest value of the *WSS* is around $1 N/m^2$, a value which does not differ significantly from the value of the *WSS* in a normal artery (without stenosis), according to Papaioannou & Stefanos, 2005 [58]. Nevertheless as the degree of the stenosis increases, the maximum value of the wall shear stress increases very much.

More precisely, in the case of the stenosis of 70% the highest value of the *WSS* is around $20 N/m^2$, meanwhile the highest value of the *WSS*, in the case of the stenosis of 90%, overpasses the value of $350 N/m^2$. The higher the value of the *WSS*, the higher the possibility of rupture of the stenosed artery.

8.5. Artery with aneurysm

In this section we deal with artery segments with aneurysms, using the same Cross type non-Newtonian model for the blood flow together with the generalized Maxwell model for the viscoelastic vessel wall. The initial and boundary conditions are the same as in the previous sections.

Abdominal Aortic Aneurysm (AAA)

To validate the model, the authors have retaken the simulations using a real case, as it can be found in the paper elaborated by Finol et al., 2002 [28], i.e., the axial-symmetric model of the abdominal aorta with a double-aneurysm as presented in figure 8.9. The length of the arterial segment is 9*cm*, the internal diameter of the normal artery is 8*mm*, the maximal internal diameter of the smaller aneurysm is 16*mm* and the maximal internal diameter of the larger aneurysm is 20*mm*. The wall thickness is 1*mm*.

The initial and boundary conditions, the values for the constants are the same as in section 2, the time integration interval being also $t \in [0,10s]$.

The mesh generated for both the fluid (blood) and solid (arterial wall) domain consists of 915 triangular elements and 39568 degrees of freedom.

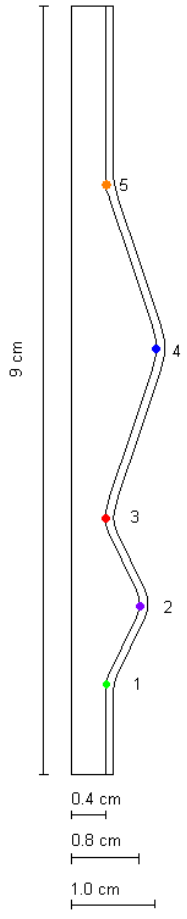

Figure 8.9 Axial-symmetric model for the Abdominal Aorta with a double aneurysm

On figure 8.10 the surface distribution of the *WSS* at t = 7.7s is presented. It can be clearly seen that the *WSS* reaches its highest absolute value at the exit point of the first ("smaller") aneurysm and at the exit point of the second ("larger") aneurysm.

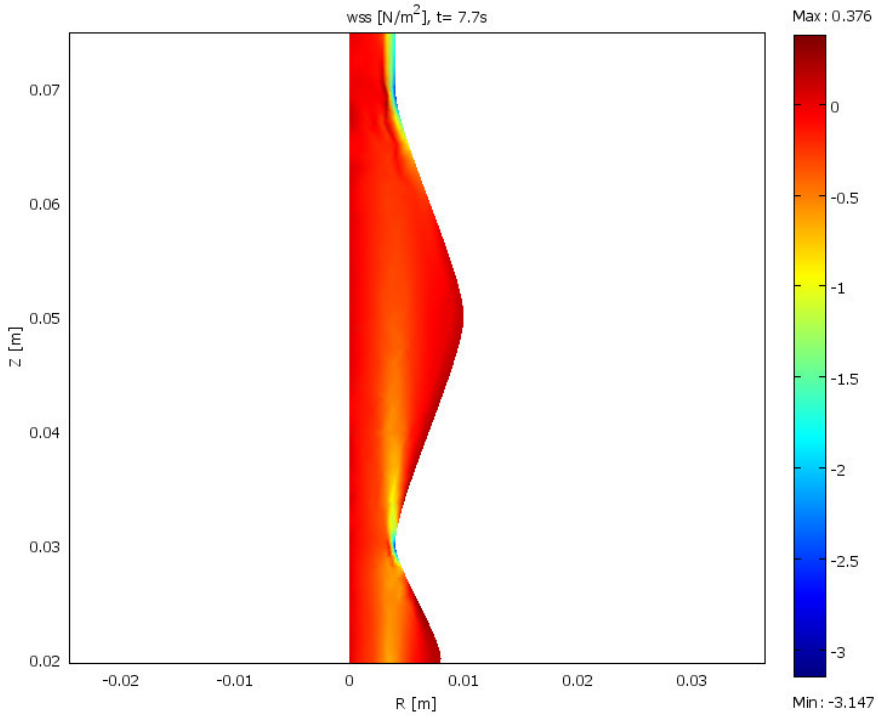

Figure 8.10 Surface distribution of the WSS in the case of AAA

8.6. *A global condition for the rupture risk of an AAA*

We intend to set up a mechanical condition whose fulfillment would lead with a high probability to the rupture of the aneurysm and consequently to the damage of the vessel wall of an *AAA*.

The above mentioned rupture takes place when the *WSS* evaluated on the boundary of aneurysm overpasses the internal cohesion forces assessed on the same boundary of the aneurysm. But these internal cohesion forces are connected with the projection of the stress vector $\vec{T}$ (Maxwell model) on the unit tangent to the boundary vector $\vec{t}$.

We accept, in a plane $\varphi = const$, that the equation of the vessel wall (with aneurysm) could be expressed in a Cartesian coordinate system formed by the radial axis $\underline{r}$ and the axis of symmetry $\underline{z}$ by the equation $z = z(r)$.

As it can be found in the paper of Albert et al. [5], using the generalized Maxwell model for viscoelastic behavior, the components of the stress vector are

$$T_r = -\left\{2G_0\left[\eta_0\left(\frac{\partial u}{\partial r}-\frac{1}{3}\left(\frac{\partial u}{\partial r}+\frac{\partial v}{\partial z}\right)\right)+A\right]-p\right\}\frac{\frac{dz}{dr}}{\sqrt{1+\left(\frac{dz}{dr}\right)^2}}+2G_0\left[\eta_0\,\frac{1}{2}\left(\frac{\partial v}{\partial r}+\frac{\partial u}{\partial z}\right)\right]\frac{1}{\sqrt{1+\left(\frac{dz}{dr}\right)^2}}$$

$$T_z = -2G_0\left[\eta_0\,\frac{1}{2}\left(\frac{\partial u}{\partial z}+\frac{\partial v}{\partial r}\right)\right]\frac{\frac{dz}{dr}}{\sqrt{1+\left(\frac{dz}{dr}\right)^2}}+\left\{2G_0\left[\eta_0\left(\frac{\partial v}{\partial z}-\frac{1}{3}\left(\frac{\partial u}{\partial r}+\frac{\partial v}{\partial z}\right)\right)+A\right]-p\right\}\frac{1}{\sqrt{1+\left(\frac{dz}{dr}\right)^2}}.$$

Then, in the points of the aneurysm boundary $z = z(r)$, the projection of the Maxwell stress vector $\vec{T}$ on the direction of the unit tangent vector to the vessel wall $\vec{t}$ will be

$$\vec{T}\cdot\vec{t} = -\left\{2G_0\left[\eta_0\left(\frac{\partial u}{\partial r}-\frac{1}{3}\left(\frac{\partial u}{\partial r}+\frac{\partial v}{\partial z}\right)\right)+A\right]-p\right\}\frac{\frac{dz}{dr}}{1+\left(\frac{dz}{dr}\right)^2}+2G_0\left[\eta_0\,\frac{1}{2}\left(\frac{\partial v}{\partial r}+\frac{\partial u}{\partial z}\right)\right]\frac{1}{1+\left(\frac{dz}{dr}\right)^2}-$$

$$-2G_0\left[\eta_0\,\frac{1}{2}\left(\frac{\partial u}{\partial z}+\frac{\partial v}{\partial r}\right)\right]\frac{\left(\frac{dz}{dr}\right)^2}{1+\left(\frac{dz}{dr}\right)^2}+\left\{2G_0\left[\eta_0\left(\frac{\partial v}{\partial z}-\frac{1}{3}\left(\frac{\partial u}{\partial r}+\frac{\partial v}{\partial z}\right)\right)+A\right]-p\right\}\frac{\frac{dz}{dr}}{1+\left(\frac{dz}{dr}\right)^2}.$$

This product would estimate the internal cohesion forces in the points of the vessel wall with aneurysm.

Concerning the wall shear stress, observing the conditions of the considered Cross law for blood, we could write

$$WSS = \left(\mu_s+\frac{\mu_0^*}{1+k\left[2\left(\frac{\partial u}{\partial r}\right)^2+2\left(\frac{\partial v}{\partial z}\right)^2+\left(\frac{\partial v}{\partial r}+\frac{\partial u}{\partial z}\right)^2+2\left(\frac{u}{r}\right)^2\right]^{\frac{1-n}{2}}}\right)\left(\frac{\partial v}{\partial r}+\frac{\partial u}{\partial z}\right).$$

The "rupture" of the vessel wall would take place if the *WSS* overpasses $\vec{T}\cdot\vec{t}$ (both considered in absolute value), i.e.,

$$\left| -\left\{ 2G_0\left[\eta_0\left(\frac{\partial u}{\partial r} - \frac{1}{3}\left(\frac{\partial u}{\partial r} + \frac{\partial v}{\partial z} \right) \right) + A \right] - p \right\} \frac{\frac{dz}{dr}}{1+\left(\frac{dz}{dr} \right)^2} + 2G_0\left[\eta_0 \frac{1}{2}\left(\frac{\partial v}{\partial r} + \frac{\partial u}{\partial z} \right) \right] \frac{1}{1+\left(\frac{dz}{dr} \right)^2} - \right.$$

$$\left. - 2G_0\left[\eta_0 \frac{1}{2}\left(\frac{\partial u}{\partial z} + \frac{\partial v}{\partial r} \right) \right] \frac{\left(\frac{dz}{dr} \right)^2}{1+\left(\frac{dz}{dr} \right)^2} + \left\{ 2G_0\left[\eta_0\left(\frac{\partial v}{\partial z} - \frac{1}{3}\left(\frac{\partial u}{\partial r} + \frac{\partial v}{\partial z} \right) \right) + A \right] - p \right\} \frac{\frac{dz}{dr}}{1+\left(\frac{dz}{dr} \right)^2} \right| <$$

$$< \left| \left(\mu_s + \frac{\mu_0^*}{1 + k\left[2\left(\frac{\partial u}{\partial r} \right)^2 + 2\left(\frac{\partial v}{\partial z} \right)^2 + \left(\frac{\partial v}{\partial r} + \frac{\partial u}{\partial z} \right)^2 + 2\left(\frac{u}{r} \right)^2 \right]^{\frac{1-n}{2}}} \right) \left(\frac{\partial v}{\partial r} + \frac{\partial u}{\partial z} \right) \right|.$$

Construction of an analytical approximation of WSS

In what follows, we intend to build up an analytical expression for approximating the *WSS* considered, at a certain moment, as a function of the *axial coordinate z*. To achieve that, we will use the numerical data of the joined table 8.1 and we interpolate the *WSS* along the whole boundary of the aneurysm.

Points	z (cm)	*WSS* (N/m^2)
1	1	-1.25
2	2	0.175
3	3	-2.55
4	5	0.16
5	7	-2.45

Table 8.1 Values of *WSS* (at a certain time t = 7.7s) at the 5 considered points as shown on figure 8.9

Our final goal is to assess the absolute minimum and maximum of *WSS* for anticipating a possible "rupture" of the vessel with aneurysm.

Denoting by $M_i = S''(z_i)$, $i = 0,1,2,3,4,5,6$ (where the point 0 and 6 correspond to the "farfield" of the aneurysm – where the deviation of the *WSS* is practically absent[1] and consequently $WSS^0 = WSS^6 = WSS'^0 = WSS'^6 = 0$), if $h_i = z_i - z_{i-1}$, the spline function joined to the "*i*" subinterval, is given by (Iacob et al., 1983 [42])

[1] Instead of the genuine complete *WSS* we will work with its "deviation" versus the normal artery (without aneurysm) and consequently the fulfillment of the required conditions is assured.

$$S_i(z)=\frac{M_i(z-z_{i-1})^3+M_{i-1}(z_i-z)^3}{6h_i}+\left(WSS^{i-1}-\frac{M_{i-1}h_i^2}{6}\right)\frac{z_i-z}{h_i}+\left(WSS^{i}-\frac{M_ih_i^2}{6}\right)\frac{z-z_{i-1}}{h_i}$$

$i=\overline{1,6}$.

Concerning the constants M_i they can be obtained by solving the following algebraic linear system

$a_0M_0+c_0M_1=d_0$

$b_iM_{i-1}+a_iM_i+c_iM_{i+1}=d_i$, $i=1,2,3,4,5$

$b_6M_5+a_6M_6=d_6$,

where $b_i=\frac{h_i}{h_i+h_{i+1}}$, $c_i=1-b_i$, $d_i=\frac{6}{h_i+h_{i+1}}\left(\frac{WSS^{i+1}-WSS^{i}}{h_{i+1}}-\frac{WSS^{i}-WSS^{i-1}}{h_i}\right)$,

$i=1,2,3,4,5$;

$b_6=1$, $c_0=1$, $d_0=\frac{6}{h_1}\left(\frac{WSS^{1}-WSS^{0}}{h_1}-WSS'^{0}\right)$, $d_6=\frac{6}{h_6}\left(WSS'^{6}-\frac{WSS^{6}-WSS^{5}}{h_6}\right)$,

$a_i=2$, $i=0,1,2,3,4,5,6$.

Concerning the error of the approximation it is of the same order as of the certain powers of $h=\max_i(z_i-z_{i-1})$, the degree of accuracy increasing together with the regularity of *WSS*.

If we want to calculate the critical points of the spline approximation for *WSS*, from

$$\frac{dS_i}{dz}=\frac{z^2(M_i+M_{i-1})-2z(z_{i-1}M_i+z_iM_{i-1})}{2h_i}+$$
$$+\frac{M_iz_{i-1}^2+M_{i-1}z_i^2+2(WSS^{i}-WSS^{i-1})-2/3h_i^3(M_i-M_{i-1})}{2h_i}$$

we have to impose the condition

$$\Delta_i=(z_{i-1}M_i+z_iM_{i-1})^2-$$
$$-(M_i+M_{i-1})\left[M_iz_{i-1}^2+M_{i-1}z_i^2+2(WSS^{i}-WSS^{i-1})-2/3h_i^3(M_i-M_{i-1})\right]\geq 0$$

The critical points, for each subinterval (z_{i-1},z_i), are given by

$$z_{1,2}^{i}=\frac{(z_{i-1}M_i+z_iM_{i-1})\pm\sqrt{\Delta_i}}{(M_i+M_{i-1})}.$$

The relative extremum values of this approximation (and implicitly of *WSS*) should be found among the values of

$$S_i(z_{1,2}^i),\ i = 1,2,3,4,5,6,$$

where we must consider only those $z_{1,2}^i \in (z_{i-1}, z_i)$ (at least approximately).

Then by considering $\min_i \left|S_i(z_{1,2}^i)\right|$ this should be the limit value of *WSS* which once overpassing the internal cohesion forces evaluated on the aneurysm boundary ($\vec{T} \cdot \vec{t}$) the rupture takes place. Of course this represents a global condition not a local one.

Concerning the projection of the stress vector ($\vec{T}$) on the boundary tangent ($\vec{t}$) using the Maxwell viscoelastic behavior for the blood walls (aneurysm included) it can be obtained also via COMSOL 3.3 [21].

In our real clinical study, the linear algebraic system was solved by QuickMath and the solutions are $M_0 = -12.447$, $M_1 = 11.395$, $M_2 = -11.085$, $M_3 = 8.045$, $M_4 = -6.352$, $M_5 = 9.383$, $M_6 = -15.067$.

Immediately we get for the critical points the coordinates (keeping those whose values are close to the inside of the considered subinterval (z_{i-1}, z_i)) $z_1 = 1.402$, $S_1(z_1) = -1.29$; $z_2 = 2.305$, $S_2(z_2) = -1.55$; $z_3 = 3.732$, $S_3(z_3) = -1.59$; $z_5 = 8.25$, $S_5(z_5) = 9.984$; $z_6 = 8.244$, $S_6(z_6) = -0.503$. Concerning $\min_i \left|S_i(z_{1,2}^i)\right|$ it is equal to 0.503.

This should be compared (after adding also 1 due to the fact that we worked with the "deviation" of WSS^2) to the maximum value of $\left|\vec{T} \cdot \vec{t}\right|$ evaluated on the boundary. As this maximum value of the internal cohesion forces (got via COMSOL Multiphysics) is 6.175, we may state that at the considered moment t = 7.7s there is no global rupture risk.

Of course these steps must be repeated at all the moments, but an appropriate soft could solve this feature without any special shortcomings.

We remark that this approach leads to a global rupture risk prediction. In our particular clinical case, in spite of the fact that *WSS* overpasses the internal cohesion forces at the point 5 (see table 8.2, where a rupture risk really exists) we may state that, globally speaking, there is no rupture risk for the considered artery.

t (s)	*WSS* (N/m^2)	$\vec{T} \cdot \vec{t}$ (N/m^2)
7.0	–0.53	–1.12
7.1	–0.58	–0.65
7.2	–0.53	–3.37
7.3	–0.77	–3.37
7.4	–0.52	+5.41
7.5	–0.66	–9.36
7.6	–2.07	–14.90
7.7	–2.94	+2.72
7.8	–0.48	–1.19
7.9	–0.39	–0.68
8.0	–0.51	–0.77

Table 8.2 *WSS* evolution in time versus the corresponding internal cohesion forces at point 5

We also remark that at point 4, where the diameter of the aneurysm is the greatest there is no risk of rupture, what implies the conclusion that the diameter of the aneurysm is not the essential parameter for the evaluation of the rupture-risk.

Bibliography

1. Agratini, O., Chiorean, I., Coman, Gh., Trîmbiţaş, R., Analiză numerică şi teoria aproximării, Vol. III, Presa Univ. Clujeană, ISBN 973-610-164-9, 2002.
2. Albert, B., Petrila, T., 2012, Mathematical Models and Numerical Simulations for the Blood Flow in Large Vessels, INCAS Buletin, Vol 4, no. 4, 3-10, 2012.
3. Albert, B., Vacaras, V., Trif, D., Petrila, T., Non-Newtonian approach of the blood flow in large viscoelastic vessels with stenosis or aneurysm, Jokull Journal, vol. 63, No. 7, pp. 160-173, 2013.
4. Albert, B., Vacaras, V., Petrila, T., Calculation of the Wall Shear Stress in the Case of an Abdominal Aortic Aneurysm, *Wulfenia*, vol. 20, No.12, pp. 159-168, 2013.
5. Albert, B., Vacaras, V., Deac, D., Petrila, T., A global condition for the rupture risk of an Abdominal Aortic Aneurysm (AAA) obtained within a mathematical and numerical model for blood flow in large vessels, acceptată spre publicare de Jokull Jornal, 2014.
6. Balan, C., Experimental and numerical investigations on the pure material instability of an Oldroyd's 3-constant model, Continuum Mech. Thermodyn., 13, 399-414, 2001.
7. Balocco, S., Basset, O., Courbebaisse, G., Boni, E., Frangi, A. F., Tortoli, P., Cachard, C., Estimation of Viscoelastic Properties of Vessel Walls Using a Computational Model and Doppler Ultrasound, Physics in Medicine and Biology, 55, No. 12, pp. 3557-3580, 2010.
8. Beavers, G.S., Joseph, D.D., Boundary conditions at a naturally permeable wall, J. Fluid Mec. 30, 1, p. 197-207, 1967.
9. Broboana, D., Muntean, T., Balan, C., Mecanica fluidelor cu FLUENT. Aplicații în dinamica biofluidelor, vol.2, ISBN 978-606-515-261-8, 2011.
10. Budwig, R., Elger, D., Hooper, H., Slippy, J., Steady Flow in Abdominal Aortic Aneurysm Models, Journal of Biomechanical Engineering, 115, pp. 418-423, 1993.

11. Calin A., Wilhelm M., Balan C., Determination of the non-linear parameter (mobility factor) of the Giesekus constitutive model using LAOS procedure, J. of Non-Newtonian Fluid Mechanics, 165, 23-24, pp. 1564-1577, 2010.
12. Carabineanu, A., Mecanică Teoretică, Editura MatrixRom, Bucuresti, 2006.
13. Chakravarty, S., Mandal, P.K., Mathematical Modelling of Blood Flow Through an Overlapping Arterial Stenosis, Mathematical and Computer Modelling, 19, pp. 59-70, 1994.
14. Chakravarty, S., Mandal, P.K., A Nonlinear Two-Dimensional Model of Blood Flow in an Overlapping Arterial Stenosis Subjected to Body Acceleration, Mathematical and Computer Modelling, 24, pp. 43-58, 1996.
15. Chakravarty, S., Mandal, P.K., Two-Dimensional Blood Flow Through Tapered Arteries Under Stenotic Conditions, International Journal of Non-Linear Mechanics, 35, 779-793, 2000.
16. Chan, W.Y., Ding, Y., Tu J.Y., Modeling of non-Newtonian blood flow through a stenosed artery incorporating fluid-structure interaction, ANZIAM Journal, 47, pp. 507-523, 2007.
17. Chen T., Determining a Prony Series for a Viscoelastic Material From Time Strain Data, NASA Center for AeroSpace Information (CASI), NASA / TM-2000-210123, pp. 1-26, 2000.
18. Cleja-Țigoiu S., Carabineanu A., Cipu C., Ionescu D., Oprea I., Stavre R., Țigoiu V., Current topics in Continuum mechanics, III. Ed. Academy, Bucharest, 2006.
19. Cleja-Țigoiu S., Țigoiu V., Reologie si termodinamica , partea I – Reologie, Ed. Universitatii din Bucuresti, 1998.
20. Cleja-Tigoiu S., Tigoiu V., An Elasto-viscoplastic Model for Complex Fluid, in New Trends in Complex Fluids Modeling, CFM2009 proceedings, Balan C., Broboana D., Kadar R., Balan C.M. (Eds.), pp. 42-44, 2009.
21. COMSOL 3.3 documentation, Nonlinear Material Model, Viscoelastic Material COMSOL documentation, file:///C:/Program%20Files/COMSOL33/doc/sme/wwhelp/wwhimpl/js/html/wwhelp.htm?context=sme&topic=viscoelastic_material

22. Craiem, C.O. Rojo, F. J., Atienza, J. M., Guinea, G. V., Armentano, R. L., Fractional Calculus Applied to Model Arterial Viscoelasticity, Latin American Applied Research, 38, 141-145, 2008.

23. Di Martino, E., Mantero, S., Inzolo, F., Melissano, G., Astore, D., Chiesa, R., Fumero, R., Biomechanics of abdominal aortic aneurysm in the presence of endoluminal thrombus: experimental characterisation and structural static computational analysis, European Journal of Vascular and Endovascular Surgery, 15, pp. 290-299, 1998.

24. Dumitrescu, H., Cardos, V., Improved formulation for Boundary-layer type flows, AIAA Journal, vol. 40, No.4, pp. 794-796, 2002.

25. Enderle, J., Susan, B. and Bronzino, B., Introduction to Biomedical Engineering. London: Academic Press, 2000.

26. Fillinger, M. F., Marra, S. P., Raghavan, M. L., Kennedy, F. E., Prediction of rupture risk in abdominal aortic aneurysm during observation: Wall stress versus diameter, Journal of Vascular Surgery, 37, No. 4, 724-732, 2003.

27. Finol E.A., Amon C.H., Flow Dynamics in Anatomical Models of Abdominal Aortic Aneurysms: Computational Analysis of Pulsatile Flow, Acta Científica Venezolana, 54, 43-49, 2003.

28. Finol, E.A., Amon, C.H., Flow-induced Wall Shear Stress in Abdominal Aortic Aneurysms: Part I – Steady Flow Hemodynamics, *Computational Methods in Biomechanics and Biological Engineering*, vol. 5, No. 4, pp. 309-318, 2002.

29. Formaggia, L., Lamponi, D. and Quarteroni, A., One-Dimensional Models for Blood Flow in Arteries, Journal of Engineering Mathematics, 47, 251-276, 2003.

30. Formaggia, L., Gerbeau, J.F., Nobile, F., Quarteroni, A., On the coupling of 3d and 1d Navier–Stokes equations for flow problems in compliant vessels, Comput. Math. Appl. Mech. Engrg., 191, pp. 561–582, 2001.

31. Fournier, R.L., Basic Transport Phenomena in Biomedical Engineering, Taylor & Francis Group, ISBN-10: 1560327081, 1998.

32. Gasser, T.C., Auer, M., Labruto, F., Swedenborg, J., Roy, J., Biomechanical rupture Risk Assessment of Abdominal Aortic Aneurysms: Model Complexity versus Predictability of Finite Element Simulations, *European Journal of Vascular and Endovascular Surgery*, 40, pp. 176-185, 2010.

33. Georgakarakos, E., Ioannou, C.V., Papaharilaou, Y., Kostas, T., Tsetis, D., Katsamouris, A.N., Peak Wall Stress Does Not Necessarily Predict the Location of Rupture in Abdominal Aortic Aneurysms, *European Journal of Vascular and Endovascular Surgery*, 39, pp. 302-304, 2010.

34. Gijsen, F.J.H., Allanic, E., Vosse, F.N. and Janssen, J.D., The Influences of the non-Newtonian Properties of Blood on the Flow in Large Arteries: Unsteady Flow in a 90 Curved Tube, Journal of Biomechanics, 32, 705-713, 1999.

35. Gineau A., Propagation of Pulsated Waves in Viscoelastic Tubes: Application in Arterial Flows, Teza de doctorat, 2010.

36. Giuma, B., Paramasivam, V., Osman, K., Kadir R.A., Muthusamy, K., Graphical User Interface (GUI) In MatLab for Solving the Pulsatile Flow in Blood Vessel, CFD Letters, 1, No. 1, 50-58, 2009.

37. Galdi, G. P., Rannacher, R., Robertson, A. M., Turek, S., Hemodynamical flows, Modeling, Analysis and Simulation, Birkhauser Verlag, ISBN 978-3-7643-7805-9, 2008.

38. Götz D., Three topics in fluid dynamics: Viscoelastic, generalized Newtonian, and compressible fluids, Verlag Dr. Hut, München, pp. 58-71, 2012.

39. Horsten, J.B.A.M., Van Steenhoven, A.A., Van Dongen, M. E. H., Linear Propagation of Pulatile Waves in Viscoelatic Tubes, Journal of Biomechanics, 22, no. 5, pp. 477-484, 1989.

40. Humphrey J. D., Delange S., An Introduction to Biomechanics, Springer, New-York, 2004.

41. Iacob, C., Introduction mathematique a la mecanique des fluides, Ed. Acad. RPR – Gauthier Villars, Paris, 1959.

42. Iacob, C., Homentcovschi, D., Marcov, N., Nicolau, A., Matematici clasice si moderne, vol. IV, Ed. Tehnica, pp. 118-122, 1983.

43. Ishikawa, T., Guimaraes, L.F.R., Oshima, S. and Yamone, R., Effect of Non-Newtonian Property of Blood on flow through a Stenosed Tube, Fluid Dynamic research, 22, 251-264, 1998.

44. Jung H., Choi J. W., Park C. G., Asymmetric flows of non-Newtonian fluids in symmetric stenosed artery, *Korea-Australia Rheology Journal*, Vol. 16, n. 2, pp. 101-108, 2004.

45. Kahaner, D., Moler, C., Nash, S., *Numerical methods and software*, Englewood Cliffs, Prentice Hall, New Jersey, pp. 97-113, 1989.

46. Lagree, P.-Y., An inverse technique to deduce the elasticiy of a large artery, Eur. Phys. J. Ap. 9, pp. 153-163, 2000.

47. Layton, W., Introduction to the Numerical Analysis of the Incompressible Viscous Flows, Computational Science & Engineering, SIAM, ISBN 978-0-898716-57-3, 2008.

48. Lazăr, D., Principiile mecanicii mediilor continue, Ed. Tehnică, 1981

49. Lee, K.W. and Xu, X.Y., Modelling of Flow and Wall Behaviour in a Mildly Stenosed Tube, Medical Engineering & Physics, 24, 575-586, 2002.

50. Marinoschi G., Functional approach to nonlinear models of water flow in soils, Mathematical Modelling Series: Theory and Applications, volume 21, Springer, ISBN 1-4020-4879-3, 2006.

51. Mandal, P.K., An Unsteady Analysis of Non-Newtonian Blood Flow through Tapered Arteries with a Stenosis, International Journal of Non-Linear Mechanics, 40, 151-164, 2005.

52. Minea, D., Hemodinamica Bifurcatiei Carotidiene, Ed. Univ. Transilvania, Brasov, ISBN 973-635-174-2, 2003.

53. Misra, J.C., Chakravarty, S., Flow in Arteries in the present of Stenosis, Journal Biomechanics, 19, 907-918, 1986.

54. Ohta, M., Wetzel, S. G., Dantan, P., Bachelet, C., Lovblad, K. O., Yilmaz, H., Flaud, P., Ruefenacht, D. A., 2005, Active Rheological Changes After Stenting of a Cerebral Aneurysm: A Finite Element Modeling, Cardiovascular and Interventional Radiology, No. 28, 768-772.

55. Oka, S., Murata, T.: A theoretical study of the flow of blood in a capillary with permeable wall, Jap. J. Appl Phys., **9**, 4, p. 345-352, 1970.

56. Oldroyd J.G., On the formulation of rheological equations of state, Proc. R. Soc. London A, 200, 523-541, 1950.

57. Olufsen, M.S., Peskin, C.S., Kim, W.Y., Pedrsen, E.M., Nadim, A., Larsen, J., Numerical Simulation and Experimental Validation of Blood Flow in Arteries with Structured-Tree Outflow Conditions, *Annals of Biomedical Engineering,* Vol. 28, pp. 1281–1299, 2000.

58. Papaioannou Th., Stefanadis, Ch., Vascular Wall Shear Stress: Basic Principles and Methods, Hellenic J. Cardiol., 46, 9-15, 2005.

59. Paulo, N., Cascarejo, J., Vouga, L., Syphilitic aneurysm of the ascending aorta, Interactive Cardiovasc Thoracic Surgery, Vol. 14, no. 2, 223-225, 2011.

60. Pedley, T. J., The Fluid Mechanics of Large Blood Vessels. Cambridge Monographs on Mechanics and Applied Mathematics. Cambridge-New York-Melbourne, Cambridge University Press, 1980.

61. Pedrizzetti, G., Domenichini, F., Fluid flow inside deformable vessels and in the left ventricle. In: Pedrizzetti G., Perktold K. (eds.) Cardiovascular fluid mechanics, Ch. 4. Springer, pp. 187-234, 2003.

62. Petrila S., Albert B., Mathematical model for the blood flow in capillary vessels, Journal of Engineering, Annals of Faculty of Engineering Hunedoara, VII, 3, pp. 352-356, 2009.

63. Petrila S., Albert B., A three dimensional axi-symmetric model for the blood flow in thin vessels, Journal of Engineering, Annals of Faculty of Engineering Hunedoara, VII, 3, pp. 357-360, 2009.

64. Petrila T., Lecţii de mecanica mediilor continue, lito, Universitatea Babeş-Bolyai, Cluj-Napoca, 1980.

65. Petrila T., Albert B., A new approach in the numerical simulation for the blood flow in large vessels, INCAS Buletin, Vol 5, no. 1, 87-93, 2013.

66. Petrila T., Albert B., Calculation of the Wall Shear Stress in the case of an Internal Carotid Artery with stenoses of different sizes, INCAS Buletin, Vol 5, Special Issue, 15-22, 2014.

67. Petrila T., Albert B., Calculation of the Wall Shear Stress in the Case of a Stenosed Internal Carotid Artery, Indian Journal of Applied Research, Vol. 3, No. 9, pp. 396-398, 2013.

68. Petrila T., Gheorghiu C.I., Metode element finit şi aplicaţii, Ed. Academiei, 1987.

69. Petrila T., Trif D., Basics of fluid mechanics and introduction to computational fluid dynamics, Springer U.S.A., 2005.

70. Petrila T., Trif D., Metode numerice şi computaţionale în dinamica fluidelor, Ed. Digital Data Cluj, ISBN 973-82011-2-8, 2002.

71. Petrusel, A., Multifuncţii şi aplicaţii, Editura Presa Universitara Clujeana, Cluj-Napoca, ISBN 973-610-060-X, 2002.

72. Pontrelli, G., Blood flow through a circular pipe with an impulsive pressure gradient, Math. Mod. & Meth. Appl. Sci., Vol. 10, no. 2, 187-202, 2000.

73. Postelnicu A., Minea Dan., Sangeorzan L., Lupu M. Modeling the hemodynamics in the human carotid artery bifurcation and computer simulation; 21st Proceedings of the International Conference on Information Technology INTERFACES ITI'99, Pula, Croatia, Junie 15-18, pp. 163-168, 1999.

74. Quarteroni, A., Modeling the Cardiovascular System – A Mathematical Adventure: Part I, SIAM News, 34, 5, pp. 1-3, 2001.

75. Quarteroni, A., Formaggia, L., Veneziani, A., The circulatory system: from case studies to mathematical modeling. In: Quarteroni, A., Formaggia, L., Veneziani, A. (eds.) Complex Systems in Biomedicine, pp.243-287, Springer, Milano, 2006.

76. Quarteroni, A., Formaggia L., Mathematical Modelling and Numerical Simulation of the Cardiovascular System, *Computational Models for the Human Body,* Handbook of Numerical Analysis Vol. XII, (Ed. N. Ayache and P.G. Ciarlet), Elsevier, Amsterdam, 2004.

77. Quarteroni, A., Ragni, S., Veneziani A., Coupling between lumped and distributed models for blood flow problems, Computing and Visualization in Science, 4, pp. 111-124, 2001.

78. Revest, M., Decaux, O., Frouget, T., Cazalets, C., Cador, B., Jégo, P., et al., Syphilitic aortitis. Experience of an internal medicine unit, Rev. Med. Intern., 27, 16-20, 2006.

79. Saito M., One-dimensional modeling of pulse wave for a human artery model, Teza de doctorat, 2010.

80. Stancu, D., Coman, Gh., Agratini, O., Trîmbiţaş, R., Analiză numerică şi teoria aproximării, Vol. I, Presa Univ. Clujeană, ISBN 973-610-043-X, 2001.

81. Stergiopulos, Young, Rogge, Computer simulation of arterial flow with applications to arterial and aortic stenoses, J. Biomechanics, 19, 12, pp. 1477-1488, 1992.

82. Sud, V. K., Sekhon, G. S., Flow through a stenosed artery subject to periodic body acceleration, *Medical & Biological Engineering & Computing*, 25, pp. 638-644, 1987.

83. Tardy, Meister, Perret, Brunner, Arditi, Non-invasive estimate of the mechanical properties of peripheral arteries from ultrasonic and photoplethysmographic measurements, *Clin. Phys. Physiol. Meas.*, Vol. 12, No. 1, pp. 39-54, 1991.

84. Taylor, C. A., Hughes, T. J.R., Zarinsb, C. K., Finite element modeling of blood flow in arteries, Computer Methods in Applied Mechanics and Engineering, 158, pp. 155-196, 1998.

85. Thiriet Marc, Biology and Mechanics of Blood Flows I: Biology, Springer, pp. 265-277, ISBN 978-0-387-74846-7, 2008.

86. Tiu C., Antochi F., Neurosonologie, Bucureşti, ISBN 973-624-375-3, pp. 106-109, 2006.

87. Trif, D., Tehnici de simulare numerica cu Matlab, Ed. Infodata, Cluj-Napoca, ISBN 978-973-88389-9-4, 2007.

88. Trif, D., Petrila, T., An almost explicit algorithm for the incompressible Navier-Stokes equations, Pure Mathematics and Applications, vol. 6, nr. 2-3, pp. 279- 285, 1995.

89. Trif D., Petrila T., An analytical-Numerical Algorithm for the Incompressible Navier-Stokes Equation in Complex Domains, in "Integral methods in science and engineering", Volume 2, pp. 206-209, C. Constanda, J. Saranen, S. Seikkala (Eds), Longman, 1997.

90. Trif, D., The Lyapunov-Schmidt method for two-point boundary value problems, Fixed Point Theory 6 (1), pp. 119-132, 2005.

91. Trif, D., LISC - a Matlab package for linear differential problems, ROMAI Journal, vol. 2, nr. 1, pp. 203-208, 2006.

92. Trîmbiţaş, R., Numericla Analysis, Cluj-Napoca University Press, 2006.

93. Trîmbiţaş, R., Numericla Analysis in MATLAB, Cluj-Napoca University Press, 2010.

94. Tu J., Yeoh G.-H., Liu C., Computational Fluid Dynamics, Butterworth-Heinemann, Elsevier, UK, ISBN 978-0-08-098243-4, pp. 12, 2013.

95. Van de Vosse, F., Van Dongen, M.E., Cardiovascular Fluid Mechanics -lecture notes, Eindhoven University of Technology, faculty of Mechanical Engineering, 1998.

96. Veneziani A., Vegara, C., An approximate method for solving incompressible Navier–Stokes problems with flow rate conditions, Computer Methods in Applied Mechanics and Engineering, 196, pp. 1685-1700, 2007.

97. Vergara C., Nitsche's Method for Defective Boundary Value Problems in Imcopressible Fluid-dynamics, J. Sci. Comput., 46, pp. 100-123, 2011.

98. Vincent J., Structural Biomaterials: Third Edition, Princeton University Press, ISBN: 9780691154008, Chapter 1, pp. 1-17, 2012.

99. Waite L., Fine J., Applied Biofluid Mechanics, The McGraw-Hill Companies, pp.187-221, 2007.

100. Womersley, J.R., Method for the calculation of velocity, rate of flow and viscous drag in arteries when the pressure gradient is known, J. Physiol., 127, pp. 553-563, 1955.

101. Zimmerman W.B.J., Multiphysics Modeling with Finite Element Methods, World Scientific Publishing, 2006.

102. Zuhaila, B. I., Mathematical Modelling of Non-Newtonian Blood Flow Through a Tapered Stenotic Artery, Phd Thesis, pp. 36-41, 2006.